https://doi.org/10.5194/egusphere-2026-1517
Preprint. Discussion started: 21 April 2026

Propagation of interplanetary (IP) shocks near the Earth

Masatoshi Yamauchi[1,*], Yoshihiro Yokoyama[2,*], Tsubasa Kotani[3], and Jügen Matzka[4]

[1]Swedish Institute of Space Physics, Kiruna, Sweden
[2]UiT, Arctic University of Norway, Tromsø, Norway
[3]Data Analysis Center for Geomagnetism and Space Magnetism, Graduate School of Science, Kyoto University, Kyoto, Japan
[4]GFZ Helmholtz Centre for Geosciences, Potsdam, Germany
[*]This author contributed equally to this work.

Correspondence: M.Yamauchi (M.Yamauchi@irf.se)

Abstract. The solar wind monitor at the Sun-Earth L1 point has been used to estimate the arrival time of interplanetary (IP) shocks associated with coronal mass ejections (CMEs) and co-rotating interaction regions (CIRs). In standard estimates, including NASA/OMNI database, the radial propagation speed of the IP shock is assumed to be the same as the measured solar wind (proton) speed, although these speeds are known to be different in both the shock theory and CME observations. To diagnose the actual error in the arrival time of the IP shocks, we statistically compared the radial propagation speed of the IP shock with the measured solar wind speed at L1. The propagation speed is obtained from the time-of-propagation between the IP shock passage at the L1 monitoring spacecraft (SOHO and ACE) and at the Earth, the latter of which is represented by the geomagnetic sudden commencement (SC). In statistics, we limited to the IP shocks with a clear geomagnetic SC signature and with velocity profiles consistent between SOHO and ACE. During 1998-2022, 375 IP shocks satisfied such conditions. For the solar wind speed, the highest value during 15 min after the IP shock passage observed by the L1 monitoring spacecraft was used. We found the following tendencies. (1) As expected, actual arrival time of the IP shock to the Earth (represented by the geomagnetic SC) is often quite different from the predicted arrival time using the L1 velocity measurement. (2) For a majority of the cases, the geomagnetic SC is observed $0-10$ min earlier than the predicted IP arrival time. (3) The speed difference is distributed asymmetrically toward faster propagation, with peak of the distribution about $+10\%$.

1 Introduction

In solar-terrestrial physics including the relevant magnetospheric physics and space weather predictions, upstream monitoring of the solar wind parameters such as the velocity, density, and the interplanetary magnetic field (IMF) is essential. The upstream measurements of these values have been continuously made at the Sun-Earth Lagrange L1 region for nearly three decades by SOHO and ACE spacecraft (recently joined by DSCOVR spacecraft). With solar wind velocity and distance between these spacecraft and the Earth, one can roughly estimate the arrival time of the coronal mass ejection (CME) and other large changes in these parameters, such as interplanetary (IP) shocks and large IMF changes.

In these estimates of the arrival time, the Earthward propagation speed of the CME and other IP shocks along the Geocentric Solar Ecliptic (GSE) coordinate $-X_{GSE}$ direction is normally assumed to be the same as the solar wind speed (anti-sunward

https://doi.org/10.5194/egusphere-2026-1517
Preprint. Discussion started: 21 April 2026

proton speed) measured at L1 (King and Papitashvili, 2026). However, the propagation speed of the IP shocks is known to be different from the solar wind speed in both the shock theory and CME observations.

In 1D shock models, the conservation of the mass flux across the shock in the shock-rest frame (Rankine-Hugoniot relation) requires that the higher-density side (solar wind after the IP shock passage) should have lower relative velocity to the shock. In the compressional (forward) shock, this condition can be achieved only if the shock speed is higher than the solar wind speed (see illustration in Appendix A for this textbook type relation). Theoretically, the shock propagation speed should be able to be derived from the measured changes in velocity and density. However, the observation of density, particularly its large increase, is often erroneous right after the IP shocks, causing such a calculated result unreliable. This is one of the reasons why the solar wind speed is used for predicting the arrival time of the IP shocks at the Earth. Furthermore, the actual IP shocks are not as ideal as simple models, and using density information might be misleading (an example is shown later).

For observation near the Sun, the CME front identified by SOHO LASCO imager sometimes propagates at velocity >1000 km/s, being much faster than the solar wind velocity measured at L1 (e.g., Manoharan et al., 2001; Yashiro et al., 2004; Tokumaru et al., 2006; Gonzalez-Esparza and Aguilar-Rodriguez, 2009). Although the CME propagation is decelerated while the solar wind is accelerated with distance from the Sun, the IP shocks propagate faster than the solar wind even near the Earth.

The time difference also comes from the different reasons. If the IP shock front surface ("phase plane") is oblique like the sector boundary along the Parker's spiral, we expect both earlier or delayed arrival of the IP shock to the Earth compared to the predicted arrival time using L1 monitor value, because the location of the monitor spacecraft (SOHO, ACE, and DSCOVR) is offset from the Sun-Earth line (Richardson and Paularena, 1998; Collier et al., 1998). This "oblique" effect can be significant because the GSE Y-Z location of the L1 monitor is normally at a large distance ($\sim 10^{5-6}$ km) away from the Sun-Earth line in the huge L1 region. Fortunately, both SOHO and ACE take nearly the symmetric orbit with respect to the Sun-Earth line (i.e., in the GSE Y-Z direction). Therefore, the statistical average of the actual arrival time is expected to converge to the expected arrival time,unlike the time difference coming from the difference in speeds.

Another possibility is when the IP shock propagates "obliquely" in the GSE Y-Z direction, like the flank side of CMEs or when a fast stream approaches the equatorial region from north or south. In such cases, the X_{GSE} component of the shock front's phase velocity will be quite different from the solar wind velocity. Fortunately, we again expect both earlier or delayed arrival of the IP shock to the Earth compared to the prediction using the solar wind speed values, and the same argument of the symmetricity above applies to the statistic.

Since the arrival time of the IP shocks to the Earth is one of the essential information in understanding the solar wind-magnetosphere interaction including the space weather prediction, it is quite important to examine the degree of difference between the radial propagation speed of IP shock (including CME) and the speed of the solar wind near the Earth. This type of difference has been reported for the transit time of the IMF changes (e.g., Collier et al., 1998; Milan et al., 2022), but less well studied for the IP shocks (e.g., Paularena et al., 1998, 1999) without statistical studies near the Earth. The purpose of this paper is statistically examine the velocity difference between the IP shock propagation and solar wind speed (accordingly, the difference in the arrival time to the Earth) using both L1 monitoring spacecraft (SOHO and ACE) and timing of the geomagnetic sudden commencement (SC), the latter of which can be used as the arrival time of the IP shock to the Earth. With very long L1

https://doi.org/10.5194/egusphere-2026-1517
Preprint. Discussion started: 21 April 2026

monitoring by SOHO (since 1996) and ACE (since 1997), there is a sufficient number of IP shocks that are identified in both spacecraft, with clear geomagnetic SC signatures.

2 Data and Method

Located at the Sun-Earth L1 point, which is about 1.5×10^6 km upstream of the Earth, SOHO and ACE monitor the upstream solar wind. The time resolution is about 30s for SOHO and 1 min for ACE in the database we used here. Technical descriptions of the solar wind monitoring instruments are found in Ipavich (1998) for SOHO and McComas et al. (1998) for ACE. Although we conventionally call L1 "point", all L1 monitoring spacecraft take the semi-periodical halo orbit around L1, which covers much larger areas than the size of the Earth (0.06×10^5 km): the distance from the L1 point in the GSE Y-Z plane can be up to 7×10^5 km for SOHO (https://soho.nascom.nasa.gov/about/orbit.html) and 3×10^5 km for ACE (https://izw1.caltech.edu/ACE/ASC/DATA/browse-html/y_z_plot.gif).

We start from the IP shock list of SOHO (https://space.umd.edu/pm/figs/history.html) and examined the velocity profile until the end of 2022. We examine both SOHO and ACE for both timing of the IP shock and the solar wind velocity. We limit the IP shock to those that are not contaminated by high-speed periods before the IP shock. Among them, we selected those that also caused a clear geomagnetic SC signature, which indicates the arrival of the IP shock to the Earth.

The geomagnetic SC is a sudden increase in the horizontal (H) component in the dayside stations that propagates quickly to the nightside (e.g., Araki, 1977; 1994). Since the propagation time of 1-3 min from the magnetopause to the Earth is about the same as the travelling time of the solar wind from the magnetopause to the Earth's terminator, we can safely use the onset time of the geomagnetic SC as a proxy of arrival time of the IP shock to the Earth (e.g., Earth's terminator).

In this method of estimating the arrival time of the IP shock, the geomagnetic variation is sometimes contaminated by on-going geomagnetic activities (this can also be examined by the geomagnetic AE index). Therefore, we also limit to the cases when the geomagnetic SC is clearly identified in SYM-H index (e.g., Nanjo et al., 2025), which is provided by WDC (https://wdc.kugi.kyoto-u.ac.jp/aeasy/index.html. This gives us 438 examples out of more than 650 IP shocks in the list. To confirm our list of the geomagnetic SC, we also used the SC list provided by the Ebre Observatory (https://www.obsebre.es/en/variations/rapid), in which the magnetometer data from five longitudinally distributed low-latitude stations are used to identify the geomagnetic SC.

2.1 Example

Fig. 1 shows one such example from the IP shock on 2006-01-01. Figs. 1a and 1b show that a sudden sharp increase in the proton speed (thick black line) and density (thin blue line) occurred simultaneously for both SOHO at 13:35 UT (Fig. 1a) and ACE at 13:30 UT (Fig. 1b). Even the total IMF strength (dashed red line) observed by ACE suddenly increased simultaneously at 13:30 UT. Since the IP shock timing was identified as a sudden increase in dynamic pressure, the above timing corresponds to the IP shock timing passing through SOHO and ACE. Fig. 1c shows that SYM-H suddenly increased at 14:05 UT as an

https://doi.org/10.5194/egusphere-2026-1517
Preprint. Discussion started: 21 April 2026

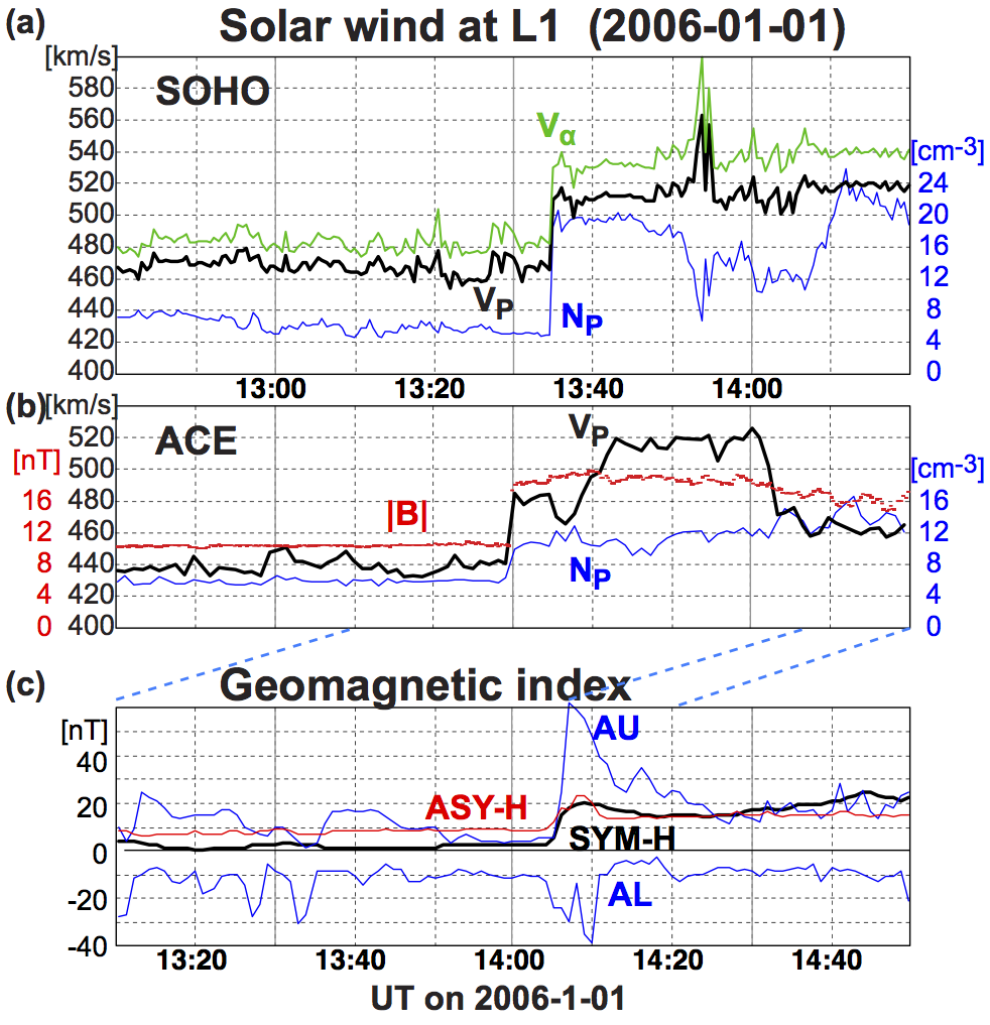

Figure 1. Solar wind data observed by (a) SOHO and (b) ACE for the IP shock event on 2006-01-01. The proton speed, proton density, and the IMF intensity are plotted by thick black lines, thin blue lines, and a thin red line, respectively. As a reference, speed of the alpha particle is also shown in (a) with a green line. The IP shock is identified as sudden simultaneous intensification of the density and velocity for both SOHO (13:35 UT) and ACE (13:30 UT). The IMF total field measured by ACE also shows sudden intensification the same timing (13:30 UT). (c) Geomagnetic indices SYM-H (thick black lines), ASY-H (thin red line), AU and AL (both thin blue lines) for the same IP. Sudden increase of SYM-H (and ASY-H and AU) is observed at 14:05 UT.

isolated geomagnetic SC during a quiet period without any contamination from any magnetospheric activities (as seen from AU and AL indices).

https://doi.org/10.5194/egusphere-2026-1517
Preprint. Discussion started: 21 April 2026

Let us estimate the propagation speed of the IP shock in the $-X_{GSE}$ direction. From the above timings, travel time of the IP shock is estimated as $dt_{soho} = 30 \pm 1$ min for SOHO-Earth propagation and $dt_{ace} = 35 \pm 1$ min for ACE-Earth propagation. We consider following two ideal cases.

(a) If the shock normal (phase plane normal) points the $-X_{GSE}$ direction, the X_{soho} distance of 1.263×10^6 km means about $\sim 700 \pm 30$ km, and $X_{ace} = 1.440 \times 10^6$ km means about $\sim 690 \pm 20$ km. Both values are consistent with each other, but much faster than the measured solar wind speed. To check this, we also estimated the propagation speed from the ACE location to the SOHO location using 5 ± 1 min time lag between these spacecraft. This gives us $\sim 590 \pm 150$ km/s along $-X_{GSE}$ direction, which is within the consistent range with the above values.

(b) If the shock front is tilted by 45° toward the Parker spiral direction, we have to take into consideration of the GSE Y location of the spacecraft (GSE $Y_{soho} = 4.69 \times 10^5$ km for SOHO and $Y_{ace} = -2.467 \times 10^5$ km for ACE). Projecting these location to GSE $Y = 0$, the X distance to the IP shock on the Sun-Earth line is estimated as 1.732×10^6 km at 13:35 UT for SOHO and as 1.193×10^6 km at 13:30 UT for ACE. These values give about $\sim 960 \pm 30$ km from the SOHO-Earth timings and $\sim 570 \pm 20$ km from the ACE-Earth timings. Meanwhile, the inter-spacecraft time lag of 5 ± 1 min also means a backward propagation with -1800 ± 450 km/s. All estimates of the propagation velocity (SOHO to the Earth, ACE to the Earth, and ACE to SOHO) contradict each other.

From (a) and (b), we can safely assume that the shock normal points nearly along the $-X_{GSE}$ direction, with the IP propagation speed of $\sim 690 \pm 20$ km. This is quite different from the maximum solar wind speed of 519 km/s (same value for both SOHO and ACE) observed within 15 min after the IP shock passage.

The derived IP shock propagation speed is even much faster than the theoretical propagation speed in a simple 1D shock model (cf. Appendix A). In the SOHO observation, the density jump across the IP shock passage is about 4 times, whereas the speed changed from 470 km/s to 520 km/s. These values lead to an estimate of 540 km/s as the propagation speed in the simple 1D shock model. On the other hand, the density jump across the shock observed by ACE is only double, i.e., much smaller than the SOHO observation, whereas the solar wind speed jumped from 440 km/s to 520 km/s, i.e., much larger than the SOHO observation. Accordingly, the estimated propagation speed in the same 1D shock model is 600 km/s.

The difference in the jump across the shock between the ACE observation and the SOHO observation might come from the instrumental difference (e.g., different saturation level) although it might reflect non-uniformity of the shock. Generally, density measurements are less reliable than the velocity measurements during high-flux events such as CME. Even if the observation is real, these theoretical propagation speeds are still much lower than the observed propagation speed (690 ± 20 km/s). This example enforces the usefulness of statistical examination of the IP shock propagation speed against the solar wind speed, both of which are direct products of the most reliable measured values rather than theoretical estimates using less reliable measurements and extra assumptions.

Next, we estimate the travel time of the IP shock from SOHO or ACE to the Earth, using the solar wind (proton) velocity right after the shock. We take the highest value of the proton speed during 15 min after the shock detection, which is 519 km/s for both SOHO and ACE. Here, we assume the shock normal (phase plane normal) points nearly in the $-X_{GSE}$ direction based on the above discussion (a) and (b).

https://doi.org/10.5194/egusphere-2026-1517
Preprint. Discussion started: 21 April 2026

The velocity value of 519 km/s predicts a travel time of 41 min from SOHO (GSE $X_{soho} = 1.263 \times 10^6$ km) to the Earth and 46 min from ACE (GSE $X_{ace} = 1.440 \times 10^6$ km) to the Earth. If we take these values as the shock propagation speed, the predicted arrival time of the same solar wind to the Earth is at 14:16 UT for both SOHO and ACE. If we take the value of 540 km/s (1D shock model applied to SOHO data, see above), the travel time reduces, but only by 2 min with a predicted arrival time of 14:14 UT. Even if we use the most likely overestimated value for ACE, the predicted arrival time is 14:10 UT, which is 5 minutes after the geomagnetic SC.

In summary, the anti-sunward propagation of the IP shock propagation on the 2006-01-01 event, which is estimated as ~ 700 km/s, is much faster than the solar wind (~ 520 km/s) or theoretical 1D shock propagation (~ 540 km/s). Accordingly, the actual IP shock arrived about 10 min earlier than the predicted arrival time based on these values ($520 - 540$ km/s).

2.2 Statistical method

Since we discuss statistics in this paper, we use only the X_{GSE} value of the spacecraft location in calculating the speed, because the error introduced by this assumption is expected to be equally distributed to plus side and minus side. We also assume that the arrival time of the IP shock to the Earth is the same as the onset time of the geomagnetic SC. With these assumptions, we can take the same procedure as the case (a) in interpreting Fig. 1: The propagation speed of the IP shock in the $-X_{GSE}$ direction ($V_{\rm IP}$) is obtained from the timings of the IP shock detection by the spacecraft and the geomagnetic SC (based on the SYM-H index), and the obtained speed is compared to the measured solar wind proton speed ($V_{\rm H}$) for which we took the highest value during 15 min after the IP shock passage. Similarly, after calculating the predicted travel time of the IP shock using the measured solar wind speed and the X_{GSE} location of the spacecraft, we obtain the difference Δt (positive for earlier arrival than prediction) from the actual propagation time using these timings.

Fig. 2 shows the distribution of Δt: left panel (a) shows a scatter plot of Δt against the predicted travel time (from SOHO to the Earth) in the X_{GSE} direction; and right panel (b) shows the number of IP shocks at different Δt. Different colors in Fig. 2 (dark blue, light blue , and orange) represent different clearness of the SC signature (see the figure caption).

Fig. 2 includes IP shocks that are quite non-uniform in the GSE Y-Z direction. In fact, the velocity profile and particularly the density profile are often different between SOHO and ACE. Although the inter-spacecraft density differences might be attributed to the different measurement methods of the solar wind protons between SOHO and ACE (ACE generally has a lower saturation level than SOHO), the inter-spacecraft difference in the velocity profile mainly comes from the non-uniform structure of the IP shock because the location difference can be as large as 3×10^5 km in the X_{GSE} direction and 8×10^5 km in the GSE Y-Z direction. This is sufficiently large in detecting the non-uniform structure of the IP shock in the GSE Y-Z direction.

In this paper, we limit to cases when the velocity profiles are consistent between SOHO and ACE with a clear IP shock signature (e.g., the velocity is relatively stable before the IP shock as mentioned above). For this, we manually examined the velocity profile. This gives us 375 "clean" examples during 1999-2022, for which we can assume that the spacecraft detected the same IP shock.

https://doi.org/10.5194/egusphere-2026-1517
Preprint. Discussion started: 21 April 2026

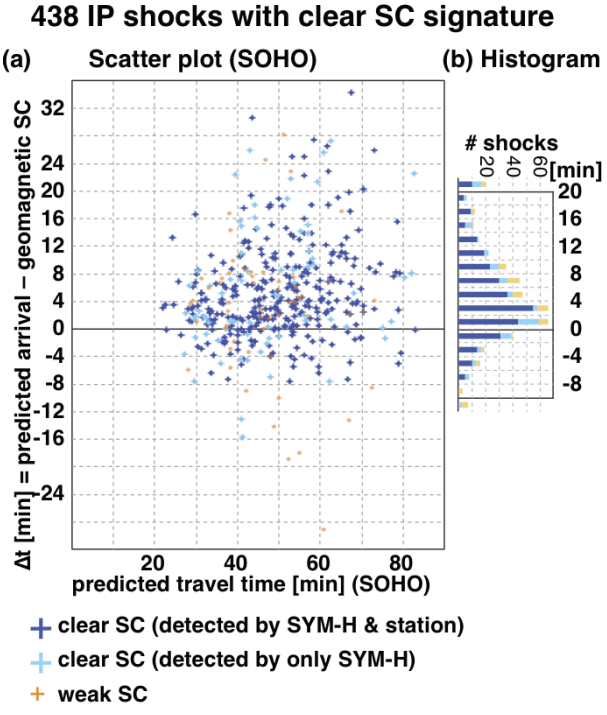

Figure 2. (a) Scatter plot of Δt against the predicted travel time in the $-X_{GSE}$ direction (from SOHO to the Earth) for 438 IP shocks in which the IP shock and geomagnetic sudden commencement (SC) are one-to-one connected. Positive Δt means that the actual arrival of the IP shock to the Earth is earlier than the predicted arrival time using the solar wind speed measured by SOHO. The data are classified into three types in terms of clearness of the SC signature: dark blue, light blue, and orange represent those when the SC is clearly identified in the SYM-H index while it is also found in the SC list at Ebre Observatory (https://www.obsebre.es/en/variations/rapid), only in the SYM-H index, and only with weak or unclear SC signatures (e.g., amplitude less than 10 nT in SYM-H index or signature during some on-going activity), respectively. (b) Histogram of the time difference Δt, which is the same as the integration of panel (a) over all the travel time. The same colors are used for the sub-classified types.

From these "clean" examples, we further filtered the IP shocks in terms of the relative timing and relative location (in X_{GSE} only) of the IP shock detection between SOHO and ACE. We first removed those when the downstream spacecraft (in terms of only X_{GSE}) detected the IP shock earlier than the upstream spacecraft. These superficially "backward" propagation indicate that the IP shock front is quite tilted in the Y direction. Accordingly, the expected arrival time of these "removed" IP shocks has some offset from the geomagnetic SC detection, in both earlier and later arrival directions. Out of 375 clean IP shocks, there are 76 such ones.

The remaining 299 IP shocks form a cleaner sub-dataset. Extending this idea, we also made another sub-dataset by limiting the superficial propagation velocity of the IP shock between two spacecraft between 250 km/s and 1500 km/s. We allow a wider speed range compared to the solar wind speed range because the inter-spacecraft time difference of the IP shock detection can

https://doi.org/10.5194/egusphere-2026-1517
Preprint. Discussion started: 21 April 2026

Table 1. Different subsets of IPs

Number of IP shocks	Cleaning level
438 "basic samples"	Clear IP shock & geomagnetic SC are identified by SOHO &SYM-H
375 "clean samples" out of 438	IP shock profile is consistent between SOHO and ACE
299 "cleaner samples" out of 375	Downstream s/c detects before upstream s/c
195 "best samples" out of 299	Shock normal most likely points in the $-X_{GSE}$ direction

be as short as 1s, with possible error of a factor of 2. There are 195 IP shocks in this category. These different levels of "cleanness" are summarized in Table 1. A list of timings of the IP shock detection and geomagnetic SC for these 438 IP shocks, including the classification of difference sub-dataset, is listed in Appendix B (Tables A1-A4).

3 Results

Fig. 3 shows the statistics of the time difference Δt for SOHO (left panels) and ACE (right panels). The format of each panel is the same as Fig. 2b. The top panels (Figs. 3a and 3d) show the distributions of all 375 clean IP shocks, the middle panels (Figs. 3b and 3e) show the distributions of cleaner subset (299 samples), and the bottom panels (Figs. 3c and 3f) show the distribution of the best subset (195 samples), as is described in the previous section.

For both SOHO and ACE, Δt values are distributed wide spread (-2 to $+12$ min for SOHO, and 0 to $+14$ min for ACE), which might indicate oblique shock front (plane normal not along the $-X$ direction). The distribution is more compact in the best dataset (Figs. 3d and 3f), i.e., less examples of extreme Δt compared to the center part (-2 min $+8$ min for SOHO) than in the original 375 clean samples (Figs. 3a and 3d). This fact indicates that filtering the dataset using the superficial inter-spacecraft propagation velocity is actually useful.

In all panels, the center of Δt is shifted toward the positive side, i.e., the IP shock generally arrives earlier than the predicted arrival time calculated from the measured solar wind speed at L1, as is expected. Furthermore, the distribution is slightly asymmetric with the positive side having a longer tail. This caused the simple average of Δt (+4s for SOHO and +6s for ACE for the best 195 IP shocks) shifting toward larger values than the most frequent Δt (+3s for SOHO and +5s for ACE). The earlier arrival of the IP shock to the Earth than the solar wind itself is valid in almost all cases, and negative Δt is most likely a part of spread of the distribution, which is expected as the statistical property of the oblique shock plane, as explained in the Introduction.

Fig. 4 shows the velocity difference, in the same format as Fig. 3. We plotted the distribution against $\log10(V_{\rm IP}/V_{\rm H})$, where $V_{\rm H}$ is the proton velocity, and $V_{\rm IP}$ is the IP shock's propagation velocity. The resultant distributions are similar to those of Δt in Fig. 3, except that the distribution for ACE is more asymmetric than Fig. 3. Otherwise, we see the same feature in $V_{\rm IP}/V_{\rm H}$ as in Δt. The propagation speed of the IP shock is about -5 to $+20\%$ faster than the solar wind speed for SOHO (0 to $+25\%$ for ACE), with the most frequently difference about 10% ($5-10\%$ for SOHO and $10-15\%$ for ACE), as shown in Figs. 4c

https://doi.org/10.5194/egusphere-2026-1517
Preprint. Discussion started: 21 April 2026

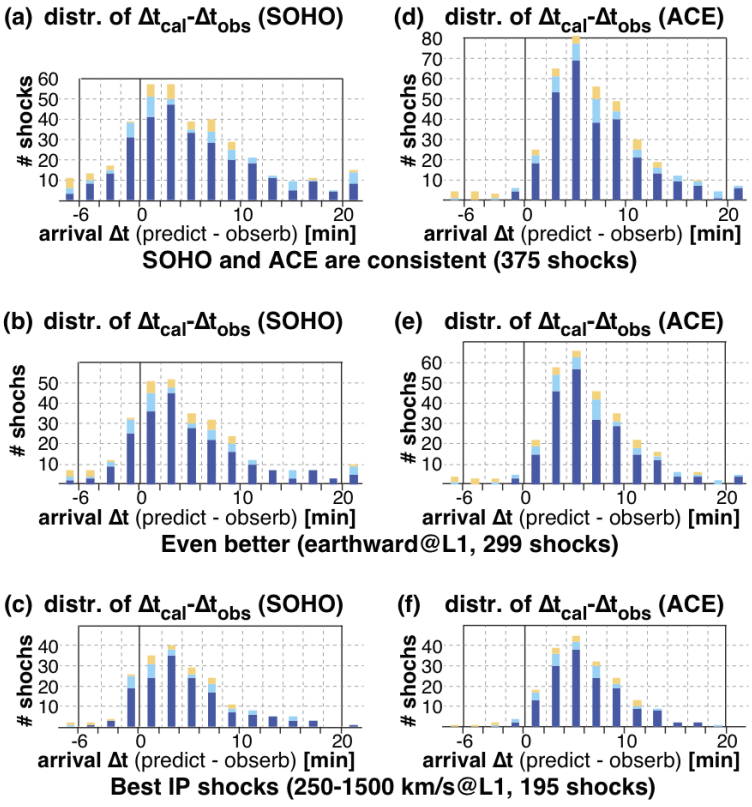

Figure 3. (a) and (d) Histogram of time difference Δt of the arrival times of the IP shock to the Earth, between the actual time using the geomagnetic sudden commencement (SC) signature seen in the SYM-H index, and the expected time using the measured solar wind velocity observed by (a) SOHO and (d) ACE. The values at both left and right edges show the summation of extreme values for both negative (< -6 min) and positive (> +20 min) sides, respectively. Positive Δt mean that the actual arrival of the IP shock to the Earth is earlier than the predicted arrival time using the solar wind speed measured by SOHO or ACE. The data are classified into three types in terms of clearness of the SC signature in the same manner as Fig. 2a. (b) and (e): The same as (a) and (d), respectively, but for those the superficial inter-spacecraft propagation direction between SOHO and ACE (assuming the sock normal points along X_{GSE}) is Earthward. (c) and (f): The same as (a) and (d), respectively, but for those the superficial inter-spacecraft propagation speed is between 250 km/s and 1500 km/s.

and 4f. The spread of $V_{\rm IP}/V_{\rm H}$ is slightly asymmetric with respect to the shifted center (most frequent ratio), with a long tail in the positive side. The simple average of $log10(V_{\rm IP}/V_{\rm H})$ for these 195 IP shocks is 0.041 (10% difference) for SOHO and 0.054 (13% difference) for ACE, which are again slightly higher than the most frequent difference, reflecting the asymmetric distribution toward the positive side.

https://doi.org/10.5194/egusphere-2026-1517
Preprint. Discussion started: 21 April 2026

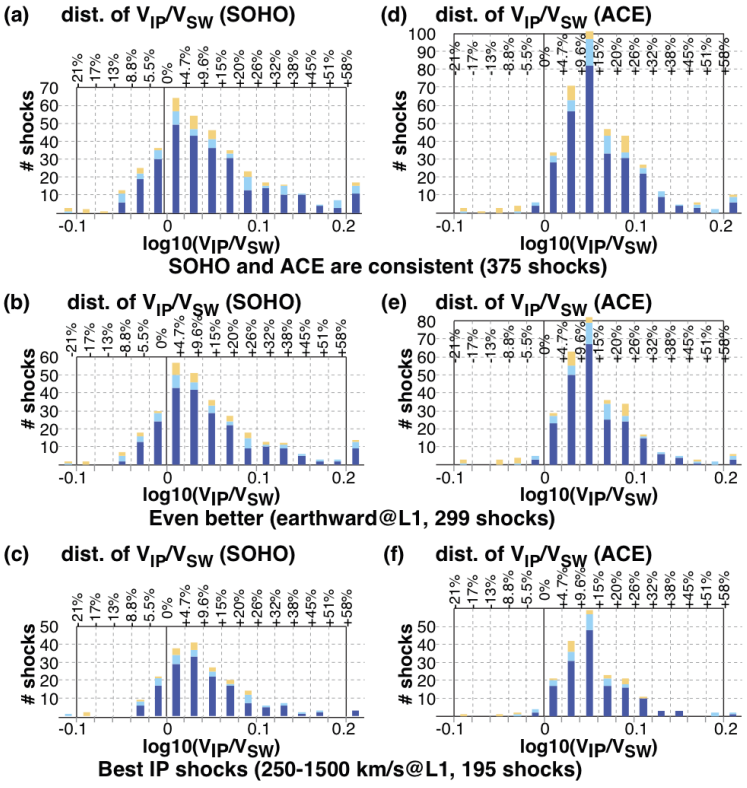

Figure 4. The same as Fig. 3, but for the velocity ratio between the solar wind proton velocity (V_H) and the IP shock's propagation velocity (V_{IP}). The latter is calculated using the time difference between the IP shock detection at L1 and the SC signature at the Earth, and the distance to the spacecraft from the Earth along the Sun-Earth line (X-direction). We plotted against $\log10(V_{IP}/V_H)$. The values at both left and right edges show the summation of extreme values for both negative (< -0.1, i.e., < 79%) and positive (> +0.2, i.e., > 158%) sides, respectively.

4 Discussion

The SOHO and ACE statistics of the IP shock during 1998-2022 shows that the geomagnetic SC takes place generally earlier than the predicted arrival time using the measured solar wind speed at L1 (highest proton speed within 15 min after the IP shock passage). The individual arrival time spreads over from about $\Delta t = -2$ to $+12$ min, with a finite number of IP shocks arrived more than 10 min earlier than the predicted time, as shown in Fig. 4c. The corresponding propagation speed of the IP shock (derived from the arrival timings of the IP shock at L1 and geomagnetic SC at the Earth) is about -5 to $+20\%$ faster than the solar wind speed for SOHO (0 to $+25\%$ for ACE), with the most frequent difference about 10% ($5-10\%$ for SOHO and $10-15\%$ for ACE), as shown in Fig. 4f.

The average differences between the IP propagation speed and the solar wind speed are consistent with the shock theory, but not all individual cases, like the example in Fig. 1. Furthermore, the spread of Δt is much longer toward large positive values

https://doi.org/10.5194/egusphere-2026-1517
Preprint. Discussion started: 21 April 2026

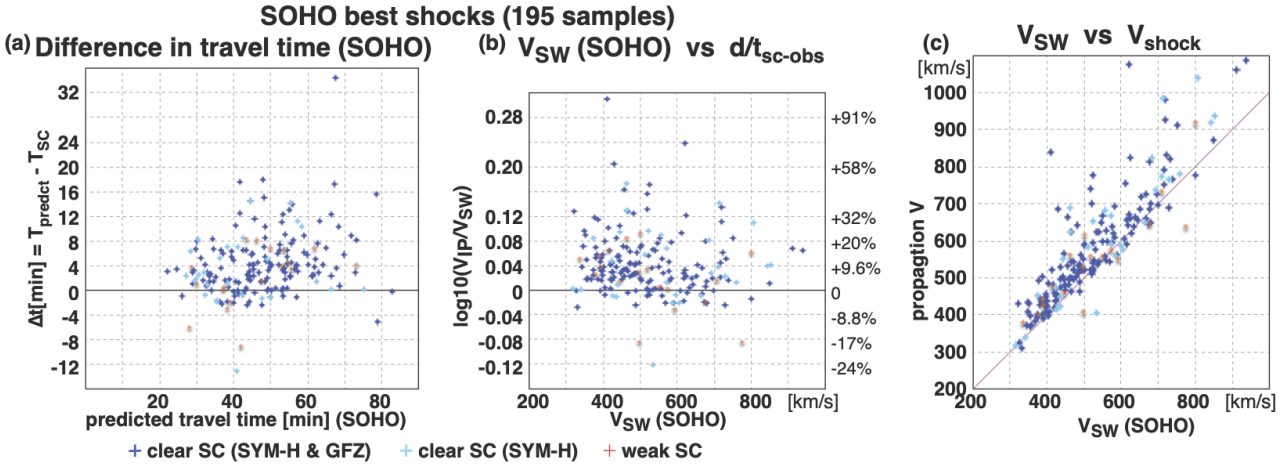

Figure 5. Scatter plot of the best 195 IP shocks in the same format as Fig. 2a: (a) Δt against the predicted travel time in the X_{GSE} direction (from SOHO to the Earth); (b) the ratio velocity log10($V_{\rm IP}/V_{\rm H}$) for SOHO observation against the solar wind velocity observed for the SOHO observation; and (c) $V_{\rm IP}$ against $V_{\rm H}$ for SOHO observation.

(earlier arrival than prediction) than toward the negative values. Therefore, it is worth examining these extreme cases in the light of shock models in future (this is outside the scope of this paper).

In the present study, the differences in the speed turned out to be only about 10% (with about 5% accuracy). For such a small differences, we must consider possible error sources in the measurements (solar wind speed and timings).

4.1 Velocity value

One obvious question is the accuracy of the velocity values. Although the SOHO proton monitor velocity is well calibrated against those measured by other SOHO instruments and other monitoring spacecraft such as Wind, with a difference less than 1% and a spread less than 3% (e.g., Ipavich, 1998), the calibration is not made during the IP shock passage when the shock speed suddenly increases. Such a saturation effect is expected most significant for ACE and SOHO, and actually the relative solar wind velocity compared the propagation velocity (Fig. 4) is smaller for the ACE observation (difference is larger) than for the SOHO observation. Can saturation occur even for SOHO?

To examine this, Fig. 5 shows the scatter plot using SOHO data (the same format as Fig. 2a) for the best 195 samples. The left panel shows Δt against the predicted travel time (corresponding to Fig. 3c), and the middle panel shows $V_{\rm IP}/V_{\rm H}$ in logarithmic scale against the measured solar wind speed by SOHO (corresponding to Fig. 4c). As reference, the scatter plot of the propagation velocity $V_{\rm IP}$ against the solar wind proton velocity $V_{\rm H}$ is shown in Fig. 5c. If the saturation of the instrument is the reason, we expect more spread for faster solar wind (longer travel time). However, Fig. 5 shows that the spread in Δt or $V_{\rm IP}/V_{\rm H}$ does not depend very much on the solar wind speed. So, the SOHO velocity observation is most likely reliable (within 1% error) even for the IP shocks that are used in this study.

https://doi.org/10.5194/egusphere-2026-1517
Preprint. Discussion started: 21 April 2026

4.2 Change of speeds from L1 to the Earth

It is quite possible that a compressional IP shock propagation is decelerated while the solar wind is accelerated, like the high-speed CME near the Sun (Yashiro et al., 2004). If the speed changes, we have to correct the solar wind speed to the average speed between L1 and the Earth, because the shock propagation speed is derived from start-end timings, and is an average value by definition. Although the velocity measurements are statistically consistent between the L1 monitoring spacecraft and the Earth orbiting spacecraft (e.g., Ipavich, 1998), the same argument as above applies here (i.e., measurements near the IP shocks can be different from relatively constant solar wind). We do not know if the distance from L1 to the Earth, which is only 1% of the distance from the Sun to the Earth, is short enough to ignore this effect. If such an acceleration is substantial, the real offset in $V_{\rm IP}/V_{\rm H}$ (and Δt) would be smaller than the present result.

4.3 Transit time from the magnetopause to the Earth

The onset timing of the geomagnetic SC was used as the proxy of the timing when the IP shock passing the Earth's terminator. Considering about 10^5 km distance from the magnetopause to the Earth, the travelling time of the IP shock (speed of about 400-900 km/s as shown in Fig. 5c) to the terminator is estimated about 1-3 min. On the other hand, the effect of the enhanced magnetopause current propagates to the Earth (to cause the geomagnetic SC) propagates with about magnetosonic speed (not the speed of light), resulting in the a similar travel time of 1-3min. Therefore, the resultant uncertainty in Δt should be, if any, only 1-2 min.

To improve the accuracy of Δt, we need to monitor the magnetopause location. The Smile satellite (Wang et al., 2025), to be launched April 2026, can monitor the magnetopause compression using soft X-ray imaging (Sambay et al., 2025). Although the instrument design is 5-min resolution, this can go down to a few minutes for strong IP shocks. Then, we may still have a better accuracy of Δt if we have many IP shocks.

4.4 Effect of the different shock front location in the GSE Y-Z direction

Since the location of ACE and SOHO are often quite away from the Sun-Earth line (up to 7×10^5 km for SOHO and 3×10^5 km for ACE) as mentioned in Sect. 2, the IP shock passage at the L1 point (on the Sun-Earth line) is generally expected to be different from the shock passage time at SOHO or ACE due to the finite tilt angle of the IP shock normal from the radial (in the $-X_{GSE}$) direction. For example, if the shock front is tilted by 45°, the difference in the passage time with 550 km/s solar wind speed can be up to ±20 min for SOHO and up to ±9 min for ACE. One possible solution minimise this uncertainty is to estimate the tilt angle of the shock normal θ in the GSE $X-Y$ plane from the relative timing of IP shock detection between two spacecraft with proper assumption of the shock plane.

By assuming a 1D plane shock with shock normal pointing within the GSE $X-Y$ plane with angle θ, the propagation speed using SOHO data should agree with that using ACE data:

$$[X_{soho} + (Y_{soho} \cdot \tan\theta)]/dt_{soho} = [X_{ace} + (Y_{ace} \cdot \tan\theta)]/dt_{ace}$$

https://doi.org/10.5194/egusphere-2026-1517
Preprint. Discussion started: 21 April 2026

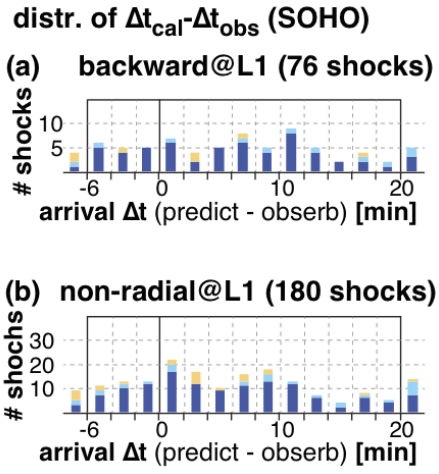

Figure 6. The same format as Figs. 3 for the removed IP shocks for SOHO. (a) Those when the spacecraft closer to the Earth in terms of the X_{GSE} direction detected earlier than the spacecraft farther away from the Earth. (b) Those removed from clean 375 IP shock when selecting the best 195 examples.

or

$$\tan\theta = -\frac{(X_{soho}/dt_{soho}) - (X_{ace}/dt_{ace})}{(Y_{soho}/dt_{soho}) - (Y_{ace}/dt_{ace})} \quad (1)$$

where dt is the time difference from the IP shock detection by the spacecraft to the geomagnetic SC, and suffix denotes the spacecraft name.

However, assumptions on the shock forms to make such "sophisticated" analyses may introduce another and significant error. For the Fig. 1 event in Sect. 2.1, Eq. (1) gives an estimate of $\theta = 6^\circ \pm 9^\circ$, and the propagation speed of IP shock as 700 ± 20 km/s (cf. our simple estimation in Sect. 2.1 was 690 ± 20 km/s). The value again contradicts the 1D model values of the shock propagation speed of 540 km/s (SOHO) and 600 km/s (ACE) using both velocity changes and density changes. Such a big difference indicates that the assumption on the shock form may not be simple. Therefore, we took different approach in the present analyses: we selected best examples for which the shock normal is expected to point more or less to the $-X_{GSE}$ direction such that this error (which is expected to show symmetric distribution in both positive and negative directions) become relatively small.

With such filtering, Figs. 3c, 3f, 4c, 4f show relatively confined distribution with shifted center. In other words, the cleaning process from the 375 clear IP shocks (Figs. 3a and 3d) to the 195 best examples (Figs. 3d and 3f) most likely removed the examples with oblique shock front (i.e., large $|\theta|$). On the other hand, the removed examples during this cleaning process should show relatively flat distribution in terms of the difference.

The result for SOHO is shown in Fig. 6. The flat distribution is consistent with the equal probability of the SOHO location in the GSE Y-Z direction (unlike more complicated ACE location) in terms of the distance from the Sun-Earth line when the IP shock front is highly oblique. The quite different distribution between the removed examples (Fig. 6) and best examples

https://doi.org/10.5194/egusphere-2026-1517
Preprint. Discussion started: 21 April 2026

(Fig. 3) also indicates that our cleaning method using the inter-spacecraft timing difference (outward speed) works in roughly selecting IP shock with the shock front lying nearly along the SG Y-Z plane.

5 Conclusions

As is expected from the shock theory, the IP shocks observed by SOHO and ACE propagate to the Earth faster than the solar wind. Using about 200 "best" IP shocks, in which the solar velocity profiles of SOHO and ACE are consistent with each other, and the shock front less likely tilts from the GSE Y-Z plane very much, we found that the time shift Δt (positive means earlier arrival than prediction) for SOHO case ranges from -2 to $+12$ min with average $+4$ min (0 to $+12$ min with average $+6$ min for ACE), as shown in Figs. 3c and 3f. These shifts correspond to about -5 to $+20\%$ faster shock propagation speed than the solar wind speed for SOHO (0 to $+25\%$ for ACE), with the most frequent difference about 10%, as shown in Figs. 4c and 4f.

Although the 10% higher speed with wide spread range in the speed ratio is not inconsistent with simple 1D shock models, the individual example (such as the case shown in Fig. 1) can be quite different between the estimation by simple shock model and the actual observation. Furthermore, the distribution of Δt (and the velocity ratio $V_{\rm IP}/V_{\rm H}$) from the shifted center is not slightly asymmetric, with the positive side more extended than the negative side.

If only one spacecraft is used, the spread of Δt is much larger than the filtered (best) case, with a substantial fraction arriving > 10 min earlier than the predicted time. This means that one must be ready for possible space weather hazard starting earlier than the predicted arrival time based on the L1 monitor.

The result also warns the usage of 1-min resolution solar wind OMNI data at the magnetopause (https://omniweb.gsfc.nasa.gov/), in which the same propagation speed as the measured solar wind speed when projecting the L1 observation to the magnetopause nose (Omniweb, 2026).

Data availability. SOHO data is taken from SOHO site (https://l1.umd.edu/) and NASA NASADCC site (https://cdaweb.gsfc.nasa.gov/). ACE data is taken from both ACE site (https://izw1.caltech.edu/ACE/ASC/level2/index.html) and NASA NASADCC site (https://cdaweb.gsfc.nasa.gov/). Geomagnetic indices are taken WDC-C2 for geomagnetism, Kyoto University (https://wdc.kugi.kyoto-u.ac.jp/wdc/Sec3.html). Another list of geomagnetic sudden commencement is found at Ebre Observatory data portal (https://www.obsebre.es/en/variations/rapid).

Appendix A: 1D-shock mass flux conservation relation

Fig. A1 illustrates the mass flux conservation relation for a textbook-type 1D compressional shock. Through conservation relation in the shock frame, the density n and velocity V in the spacecraft frame has a relation of

$$n_a \cdot (V_{sh} - V_a) = n_b \cdot (V_{sh} - V_b)$$

https://doi.org/10.5194/egusphere-2026-1517
Preprint. Discussion started: 21 April 2026

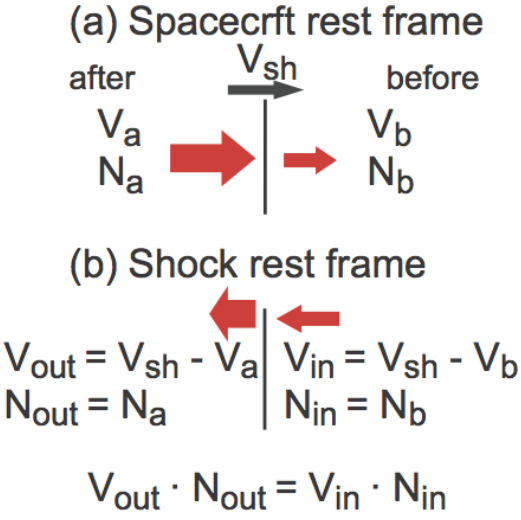

Figure A1. Illustration of mass flux ($n \cdot v$, where n is density and v is 1D speed) conservation across a 1D shock in (a) spacecraft rest frame and (b) shock rest frame. Suffix "a", "b", and "sh" in the upper panel denote after the shock passage, before the shock passage, and shock front, respectively. Suffix "in" and "out" in the lower panel denote the inflow to the shock and outflow from the shock, respectively.

or

$$(V_{sh}/V_a) = \frac{1-\epsilon\cdot(V_b/V_a)}{(1-\epsilon)} \quad \text{(A1)}$$
$$> 1 \ \text{(for compressional shock)}$$

where $\epsilon = (n_b/n_a) < 1$, and suffix "a", "b", and "sh" denote after the shock passage, before after the shock passage, and shock front, respectively.

Appendix B: Timing list of IP shocks

Table A1 lists the timings of the best 195 IP shocks (see Table 1) that was used in making Figs.3c, 3f, 4c, and 4f. The second and third columns show the UTs of IP shock detection by SOHO and by ACE, respectively. The fourth column shows the onset UT of sudden increase of SYM-H. The last column indicates the clearness of the SC (see caption of Fig. 2).

In the same format, Table A2 lists the timings of the remaining 104 IP shocks other than the best 195 shocks (after removing the samples listed in Table A1) out of 299 "cleaner" IP shock in Table 1. This subset is used in making Figs 6b.

Similarly, Table A3 lists the timings of the remaining 76 IP shocks (after removing the samples listed in Tables A1 and A2) out of 375 "clean" IP shock on Table 1. This subset is used in making Figs 6a.

Finally, Table A4 lists the timings of the 63 IP shocks with only SOHO data (after removing the samples listed in Tables B1, B2, and B3) out of 438 "basic samples" IP shock in Table 1.

https://doi.org/10.5194/egusphere-2026-1517
Preprint. Discussion started: 21 April 2026

Author contributions. MY and YY initiated the work. YY made overview plots related to SOHO and ACE in several format for all the events, and prepared tables that contain the velocity, timing, and the expected transit time. MY made the sub-dataset of the geomagnetic SYM-H indices (SYMASY) to identify the onset timing of geomagnetic SC timing, and examined all these plots to revise and complete the table made by YY. TK mainly contributed to SYM-H part, and JM made independent SC list from different dataset. MY made first draft of the text and figures, while all others contributed the text and discussion.

Competing interests. The authors declare that they have no competing interests.

Acknowledgements. SOHO is a project of international cooperation between ESA and NASA. ACE is a NASA project that is aimed as the solar wind monitor during the International Solar Terrestrial Program. Data from both spacecraft are open access. The authors gratefully thank the instrument teams that maintained the quality of the solar wind data at L1 for nearly 30 years that are used in this study: SOHO PM team (PI: F.M. Ipavich), ACE SWEPAN team (PI: D.J McComas), and ACE MG team (PI: N. Ness). The NASA OMINI data at Omniweb site is maintained by Space Physics Data Facility, NASA Goddard Space Flight Center.

Geomagnetic indices SYMASY and AE are calculated by World Data Center (WDC) for Geomagnetism, Kyoto using geomagnetic field data at SYMASY stations (San Juan, Fredericksburg, Boulder, Tucson, Papeete, Honolulu, Memambetsu, Urumqi, Alma Ata, Alibag, Martin de Vivies, Hermanus, Chambon-la-Foret) and AE stations (Abisko, Amderma, Dixon Island, Cape Chelyuskin, Tixie Bay, Pebek, Cape Wellen, Barrow, College, Yellowknife, Fort Churchill, Sanikiluaq, Great Whale River, Poste-de-la-Baleine, Narsarsuaq, Leirvogur). The geomagnetic SC list at Ebre Observatory (https://www.obsebre.es/en/variations/rapid) is derived from geomagnetic field data at many stations listed there. We thank all these contributing observatories.

Special thank goes to T. Araki (diseased August 2025) who initiate another work for which the produced plots lead this work. Without him, we never started this work. MY is partly supported by Swedish National Space Agency (dnr 2024-00124).

https://doi.org/10.5194/egusphere-2026-1517
Preprint. Discussion started: 21 April 2026

References

Araki, T.: Global structure of geomagnetic sudden commencements, Planet. Space Sc., 25, 373?384, https://doi.org/10.1016/0032-0633(77)90053-8, 1977.

Araki, T.: A Physical Model of the Geomagnetic Sudden Commencement, 183-200, American Geophysical Union (AGU), ISBN 9781118663943, https://doi.org/10.1029/GM081p0183, 1994.

Collier, M.R., Slavin, J.A.,, Lepping, R.P., Szabo, A., and Ogilvie, K.: Timing accuracy for the simple planar propagation of magnetic field structures in the solar wind, Geophys. Res. Lett., 25, 2509-2512, https://doi.org/10.1029/98GL00735, 1998.

Gonzalez-Esparza, A. and Aguilar-Rodriguez, E.: Speed evolution of fast CME/shocks with SOHO/LASCO, WIND/WAVES, IPS and in-situ WIND data: analysis of kilometric type-II emissions, Ann. Geophys., 27, 3957–3966, https://doi.org/10.5194/angeo-27-3957-2009, 2009.

Ipavich, F.M., Galvin, A.B., Lasley, S.E., Paquette, J.A., Hefti, S., Reiche, K.U., et al.: Solar wind measurements with SOHO: The CELIAS/MTOF proton monitor J. Geophys. Res., 103, 17205-17213 https://doi.org/10.1029/97JA02770, 1998.

King, J., and Papitashvili, N.: Explanation of one min and 5-min solar wind data sets at the Earth's bow shock nose of OMNIWeb, https://omniweb.gsfc.nasa.gov/html/omni_min_data.html#3, (last access, 12 February 2026), 2025.

Manoharan, P.K., Tokumaru, M., Pick, M., Subramanian, P., Ipavich, F.M., Schenk, K., Kaiser, M.L., Lepping, R.P., and Vourlidas. A.: Coronal mass ejection of 2000 July 14 flare event: Imaging from near-Sun to Earth environment, Astrophys. J., 559, 1180-1189, https://doi.org/10.1086/322332, 2001.

McComas, D.J., Bame, S.J., Barker, P., Feldman, W.C., Phillips, J.L., Riley, P., and J.W. Griffee J.W.: Solar Wind Electron Proton Alpha Monitor (SWEPAM) for the Advanced Composition Explorer, Space Sci. Rev. 86, 563–612, https://doi.org/10.1023/A:1005040232597, 1998.

Milan, S.E., Carter, J.A., Bower, G.E., Fleetham, A.L., and Anderson, B.J.: Influence of off-Sun-Earth line distance on the accuracy of L1 solar wind monitoring, J. Geophys. Res., 127, e2021JA030212, https://doi.org/10.1029/2021JA030212, 2022

Nanjo, S., Yamauchi, M., Johnsen, M.G., Yokoyama, Y., Brändström, U., Ogawa, Y., Willer, A.N., and Hosokawa, K.: Leaping and vortex motion of the shock aurora toward the late evening sector observed on 26 February 2023, Ann. Geophys., 43, 303-317, https://doi.org/10.5194/angeo-43-303-2025, 2025.

NASA Goddard Space Flight Center: Omniweb Plus https://omniweb.gsfc.nasa.gov/, (last access, 12 February 2026), 2026.

Paularena, K.I., Richardson, J.D., Zastenker, G.N., Dalin, P.A.: Solar wind correlations: Using a solar wind monitor successfully, In: Sibeck, D.G., Kudela, K. (eds) Interball in the ISTP Program. NATO Science Series, vol 537. Springer, Dordrecht. https://doi.org/10.1007/978-94-011-4487-2_12, 1999.

Paularena, K.I., Zastenker, G.N., Lazarus, A.J. and Dalin, P.A.: Solar wind plasma correlations between IMP 8, INTERBALL-1 and WIND, J. Geophys. Res., 103, 14601-14617, https://doi.org/10.1029/98JA00660, 1998.

Richardson J.D., and Paularena, K.I.: The orientation of plasma structure in the solar wind, Geophys. Res. Lett., 25, 2097-2100, https://doi.org/10.1029/98GL01520, 1998.

Sembay, S., Cheney, A., Hampson, R., et al., The soft X-ray imager (SXI) on the SMILE Mission, Space Sci. Rev. 221, 113, https://doi.org/10.1007/s11214-025-01241-y, 2025.

Tokumaru, M., Kojima, M., Fujiki, K., and Yamashita, M.: Tracking heliospheric disturbances by interplanetary scintillation, Nonlin. Processes Geophys., 13, 329–338, https://doi.org/10.5194/npg-13-329-2006, 2006.

https://doi.org/10.5194/egusphere-2026-1517
Preprint. Discussion started: 21 April 2026

Wang, C., Branduardi-Raymont, G., Escoubet, C.P., and Forsyth, C.: Solar wind magnetosphere ionosphere link explorer (SMILE): Science and mission overview, Space Sci. Rev. 221, 9, https://doi.org/10.1007/s11214-024-01126-6, 2025.

Yashiro, S., Gopalswamy, N., Michalek, G., St. Cyr, O.C., Plunkett, S.P., Rich, N.B., and Howard, R. A.: A catalog of white light coronal mass ejections observed by the SOHO spacecraft, J. Geophys. Res., 109, A07105, https://doi.org/10.1029/2003JA010282, 2004.

https://doi.org/10.5194/egusphere-2026-1517
Preprint. Discussion started: 21 April 2026

Table A1: Timing of IP detection and geomagnetic SC for best 195 samples

Date	SOHO	ACE	SYM-H	SC[*1]
19980407	16:58	16:51	17:51	both
19980501	21:14	21:22	21:57	both
19980529	14:58	15:03	15:38	both
19981107	07:34	07:37	08:16	both
19990310	00:45	00:40	01:31	both
19990505	14:45	14:59	15:43	both
19990517	23:53	24:03	24:57	both
19990626	19:26	19:25	20:17	both
19990706	14:22	14:17	15:10	both
19990804	01:30	01:16	02:20	both
19990815	09:51	09:38	10:44	both
19991021	01:33	01:38	02:26	both
19991028	11:16	11:27	12:16	both
19991105	19:07	19:14	20:10	both
20000111	13:51	13:40	14:27	both
20000127	14:13	13:56	14:53	both
20000205	15:00	14:48	15:44	both
20000211	02:21	02:13	02:59	both
20000211	23:23	23:18	23:53	both
20000214	07:07	06:56	07:33	both
20000220	20:56	20:46	21:40	both
20000406	16:01	16:04	16:40	both
20000623	12:33	12:27	13:03	both
20000713	09:10	09:01	09:43	both
20000719	15:00	14:47	15:26	both
20000726	18:08	17:55	18:57	both
20000728	05:53	05:42	06:34	both
20000811	18:18	18:11	18:46	both
20000906	16:18	16:13	17:01	both
20001005	02:35	02:40	03:26	both
20001012	21:35	21:44	22:28	both
20001028	09:00	09:08	09:55	both
20001031	16:22	16:30	17:15	both
20001104	01:29	01:34	02:21	both
20001106	09:06	09:15	09:49	both
20010110	15:28	15:19	16:21	both
20010117	15:45	15:31	16:32	both
20010123	10:15	10:06	10:49	both
20010131	07:35	07:22	08:05	both
20010331	00:14	00:23	00:52	both
20010408	10:23	10:32	11:02	both
20010411	13:02	13:14	13:44	both
20010413	07:05	07:13	07:35	both
20010417	23:56	24:05	24:47	both
20010421	14:57	15:06	16:01	both
20010428	04:28	04:31	05:00	both
20010527	14:17	14:18	14:59	both
20010803	06:37	06:25	07:16	both
20010817	10:26	10:16	11:03	both
20010929	09:03	09:05	09:39	both
20010930	18:41	18:46	19:25	both
20011011	16:12	16:20	17:01	both
20011021	16:05	16:12	16:47	both
20011025	07:57	08:02	08:50	both
20011028	02:33	02:43	03:19	both
20011031	12:49	12:53	13:49	both
20011115	13:45	13:53	15:09	both
20011119	17:34	17:35	18:15	both
20011229	04:56	04:47	05:38	both
20011230	19:39	19:32	20:10	both
20020131	20:44	20:38	21:26	both
20020318	12:32	12:36	13:21	both
20020320	13:04	13:06	13:28	both
20020323	10:46	10:53	11:36	both
20020329	21:27	21:40	22:37	both
20020417	10:13	10:21	11:07	both
20020419	07:58	08:02	08:35	both
20020423	04:07	04:15	04:49	both
20020719	09:36	09:32	10:09	both
20020725	13:03	12:59	13:37	both
20020729	12:43	12:40	13:22	both
20020801	22:30	22:20	23:11	both
20020818	18:15	18:10	18:46	both
20020930	07:13	07:21	08:16	both
20030408	00:04	00:15	01:12	both
20030618	04:44	04:29	05:13	both
20040122	01:10	01:04	01:36	both
20040403	08:49	08:56	09:48	both
20040412	17:34	17:36	18:17	both
20040726	22:28	22:26	22:49	both
20040913	19:29	19:34	20:02	both
20041107	17:59	17:53	18:27	both
20041205	07:04	06:55	07:47	both
20050528	03:47	03:31	04:37	both
20050529	09:15	09:03	09:53	both
20050612	06:58	06:51	07:46	both
20050710	02:56	02:47	03:38	both
20050824	05:33	05:38	06:13	both
20050902	13:32	13:40	14:20	both
20050909	13:10	13:16	14:01	both
20050915	08:25	08:29	09:05	both
20060101	13:35	13:29	14:05	both
20060428	00:20	00:11	01:18	both
20060819	10:39	10:50	11:32	both
20061214	13:56	13:52	14:15	both
20080528	01:32	01:28	02:25	both
20090528	04:21	04:16	05:20	both
20091004	03:15	03:07	04:14	both
20100402	06:45	06:35	07:16	both
20100405	07:59	07:54	08:27	both
20100411	12:18	12:13	13:04	both
20100803	16:51	16:55	17:41	both
20110329	15:13	15:01	16:03	both
20110418	06:06	05:56	06:52	both
20110711	08:05	08:10	08:50	both
20110909	11:49	11:42	12:43	both
20110917	03:05	02:55	03:44	both
20110926	12:02	11:52	12:35	both
20111005	06:55	06:46	07:37	both

https://doi.org/10.5194/egusphere-2026-1517
Preprint. Discussion started: 21 April 2026

20111024	17:50	17:48	18:31	both
20120307	03:47	03:35	04:20	both
20120312	08:45	08:42	09:15	both
20120315	12:42	12:35	13:08	both
20120423	02:29	02:27	03:21	both
20120616	08:52	08:57	09:56	both
20120616	19:24	19:30	20:20	both
20120903	11:33	11:22	12:14	both
20120930	22:21	22:13	23:07	both
20121031	14:46	14:39	15:40	both
20130216	11:12	11:10	12:10	both
20130315	04:46	04:40	05:27	both
20130317	05:34	05:27	06:01	both
20130627	13:45	13:52	14:39	both
20130820	21:43	21:33	22:29	both
20131002	01:24	01:18	01:56	both
20131213	12:01	12:08	13:24	both
20140107	14:24	14:25	15:14	both
20140220	02:58	02:51	03:20	both
20140227	16:17	16:07	16:51	both
20140503	16:50	16:49	17:48	both
20140911	23:02	22:57	23:45	both
20141223	10:30	10:33	11:16	both
20150317	04:10	04:03	04:45	both
20150815	07:49	07:44	08:30	both
20150920	05:32	05:27	06:05	both
20151106	17:32	17:34	18:19	both
20151219	15:27	15:28	16:17	both
20160719	23:09	23:03	23:51	both
20170831	04:49	04:44	05:39	both
20170906	23:13	23:08	23:45	both
20170907	22:38	22:35	23:01	both
20190510	16:50	16:53	17:55	both
20190708	18:38	18:30	19:23	both
20190727	08:12	08:07	09:09	both
20210827	00:28	00:24	01:16	both
20211227	08:51	08:41	09:37	both
20220201	21:42	21:36	22:22	both
20230315	03:42	03:48	04:28	both
19990221	21:52	21:46	22:41	symH
19990815	18:47	18:35	19:38	symH
20000711	08:22	08:17	09:16	symH
20000713	09:32	09:19	09:54	symH
20000814	21:48	21:36	22:19	symH
20010113	01:50	01:43	02:20	symH
20010327	01:03	01:09	01:44	symH
20010411	15:18	15:27	15:48	symH
20010818	05:37	05:24	06:14	symH
20020110	15:52	15:44	16:20	symH
20021002*2	22:08	22:14	22:55	symH
20021224	13:18	13:14	13:55	symH
20030530	16:02	15:53	16:24	symH
20030620	08:04	07:56	08:37	symH
20041109	18:24	18:20	18:49	symH
20050217	22:00	22:04	22:46	symH
20060818	15:41	15:49	16:42	symH
20071112	21:37	21:26	22:21	symH
20090114	00:05	00:13	01:20	symH
20110929	00:27	00:20	01:04	symH
20111030	08:56	08:54	10:02	symH
20120904	22:12	22:03	22:46	symH
20120912	20:17	20:04	21:05	symH
20130525	09:06	09:09	09:49	symH
20130623	03:53	03:56	04:27	symH
20150302	02:47	02:37	03:18	symH
20151104	03:22	03:23	03:54	symH
20220615	04:07	04:00	04:35	symH
20220723	02:30	02:26	02:58	symH
19980218	08:01	07:53	08:44	weak
19990228	20:46	20:33	21:32	weak
19990823	11:38	11:29	12:24	weak
19991113	12:04	12:13	12:55	weak
20000726	03:02	02:53	03:52	weak
20000728	09:19	09:09	09:57	weak
20001028	05:31	05:41	06:40	weak
20021219	13:31	13:17	14:22	weak
20030529	18:36	18:30	19:01	weak
20030703	13:16	13:09	13:53	weak
20030717*2	00:13	00:08	00:42	weak
20030727*2	04:42	04:38	05:16	weak
20041205	04:16	04:06	05:11	weak
20041211	13:03	12:57	13:40	weak
20110623	02:18	02:24	02:59	weak
20140219	03:14	03:09	03:49	weak
20170716	16:58	16:53	17:39	weak
20210424	22:16	22:22	23:05	weak

*1: Identification of geomagnetic SC by both methods (=2), by only SYM-H (=1), and weak/unclear SC (=?)
*2: Reverse (rarefied) shock

https://doi.org/10.5194/egusphere-2026-1517
Preprint. Discussion started: 21 April 2026

Table A2 Timing of IP detection and geomagnetic SC for better 104 samples

Date	SOHO	ACE	SYM-H	SC[*1]
19980423	17:13	17:28	18:25	both
19980515	13:41	13:57	14:52	both
19980613	18:25	18:55	19:26	both
19990626	02:35	02:18	03:25	both
19991212	15:14	15:14	15:52	both
20000604	14:17	14:23	15:02	both
20001002	23:58	24:08	24:54:	both
20001128	04:47	04:57	05:31	both
20010303	10:52	10:40	11:22	both
20010319	10:12	10:22	11:14	both
20010322	12:32	12:42	13:42	both
20010327	17:02	17:15	17:47	both
20010404	14:20	14:22	14:54	both
20010914	01:07	01:18	02:05	both
20020511	09:16	09:25	10:14	both
20020520	02:56	02:57	03:41	both
20020523	10:17	10:14	10:50	both
20020717	15:29	15:26	16:03	both
20020801	04:44	04:24	05:11	both
20021126	21:21	21:10	21:51	both
20030529	11:52	11:51	12:25	both
20031024	14:47	14:48	15:25	both
20031104	05:53	05:58	06:26	both
20031115	05:27	05:18	05:50	both
20031120	07:28	07:27	08:03	both
20040409	01:47	01:49	02:33	both
20040410	19:25	19:26	20:10	both
20040730	20:41	20:31	21:14	both
20041107	02:22	01:53	02:57	both
20041107	10:22	09:58	10:53	both
20050121	16:48	16:47	17:11	both
20060709	21:04	20:46	21:37	both
20061216	17:43	17:22	17:56	both
20070507	07:48	07:25	08:27	both
20070927	10:52	10:52	11:52	both
20071025	10:56	10:38	11:35	both
20090903	14:54	14:46	15:53	both
20091021	23:25	23:07	24:18	both
20110214	15:02	14:56	15:57	both
20110218	00:40	00:40	01:31	both
20110604	19:45	19:58	20:45	both
20111128	21:27	21:15	21:51	both
20120226	21:07	20:56	21:40	both
20120521	18:52	18:44	19:38	both
20120616	20:29	20:30	21:16	both
20120720	04:00	04:16	04:49	both
20120721	15:25	15:34	16:13	both
20130119	16:34	16:46	17:34	both
20130413	22:24	22:13	22:54	both
20130518	00:23	00:23	01:11	both
20130519	22:13	22:20	23:09	both
20131008	19:51	19:40	20:21	both
20140207	16:28	16:17	17:06	both
20140607	15:57	16:08	16:53	both
20140623	22:00	22:01	23:08	both
20140714	13:27	13:28	14:32	both
20140819	06:14	05:58	06:59	both
20140912	15:27	15:26	15:54	both
20141110	01:31	01:36	02:21	both
20141221	18:22	18:23	19:12	both
20150506	00:50	00:53	01:43	both
20161012	21:25	21:19	22:13	both
20161109	05:28	05:34	06:44	both
20170527	14:27	14:39	15:34	both
20170708	23:27	23:13	24:11	both
20170716	05:18	05:17	06:00	both
20170914	10:19	10:18	11:16	both
20180108	05:59	05:52	06:47	both
20180215	08:06	07:50	08:37	both
20180419	22:59	23:10	24:22	both
20190526	21:01	21:09	22:15	both
20210512	05:45	05:49	06:39	both
20210526	11:53	11:45	12:45	both
20000915	04:14	03:59	04:49	symH
20010104	13:07	13:06	14:02	symH
20010407	16:44	16:58	17:33	symH
20011001	21:15	21:29	22:02	symH
20020322	03:22	03:23	04:07	symH
20030509	04:49	04:56	05:20	symH
20031207	14:01	13:41	14:18	symH
20040801	02:02	01:49	02:28	symH
20090624	09:45	09:51	11:02	symH
20120121[*2]	03:49	04:00	05:02	symH
20120222[*2]	01:34	01:24	02:16	symH
20120520	01:44	01:37	02:15	symH
20121126	04:32	04:36	05:14	symH
20150325	09:21	09:06	09:58	symH
20151024	18:39	18:27	18:56	symH
20200630	01:35	01:23	02:17	symH
19981108	04:19	04:21	04:52	weak
20010802	14:27	14:06	15:11	weak
20020315	18:00	18:26	19:21	weak
20020907	15:53	16:09	16:37	weak
20050131	09:58	09:50	10:22	weak
20060413	11:41	11:12	12:04	weak
20120102	00:44	00:59	01:52	weak
20130602[*2]	01:57	02:10	02:26	weak
20130903	17:02	16:46	17:45	weak
20140810	21:39	21:26	22:31	weak
20141228[*2]	22:02	22:08	22:57	weak
20150201	06:10	06:01	06:39	weak
20150223	22:01	21:49	22:47	weak
20170520[*2]	08:49	08:49	09:23	weak
20190404	13:06	13:08	14:09	weak

*1: Identification of geomagnetic SC by both methods (=2), by only SYM-H (=1), and weak/unclear SC (=?)
*2: Reverse (rarefied) shock

https://doi.org/10.5194/egusphere-2026-1517
Preprint. Discussion started: 21 April 2026

Table A3 Timing of IP detection and geomagnetic SC for very oblique 76 samples

Date	SOHO	ACE	SYM-H	SC[*1]
19980503	17:05	17:00	17:44	both
19980508	09:23	09:21	09:52	both
19990416	10:46	10:35	11:26	both
19990702	00:22	00:24	01:00	both
19990712	01:09	01:15	02:20	both
19990912	03:14	03:20	04:00	both
20000608	08:42	08:41	09:10	both
20000710	05:55	05:57	06:39	both
20001126	11:25	11:23	11:58	both
20010618	01:53	01:54	03:00	both
20010812	10:48	10:48	11:35	both
20010827	19:14	19:19	19:53	both
20020217	01:56	02:09	02:55	both
20020228	03:49	04:03	04:51	both
20020510	10:28	10:29	11:24	both
20020518	19:29	19:19	20:08	both
20020530	01:25	01:32	02:05	both
20021109	17:56	17:55	18:50	both
20030320	04:21	04:20	04:44	both
20030817	13:38	13:41	14:22	both
20031026	18:35	18:31	19:09	both
20040722	09:45	09:54	10:37	both
20040829	09:20	09:17	10:06	both
20041109	09:05	09:14	09:31	both
20050727	18:43	18:49	19:39	both
20070920	09:26	09:05	10:13	both
20071217	02:02	02:04	02:53	both
20080624	19:08	19:18	20:11	both
20081124	22:47	22:48	23:52	both
20090303	04:53	04:51	06:03	both
20110310	05:45	06:08	06:34	both
20110610	08:11	08:07	08:48	both
20110617	02:05	02:01	02:40	both
20110804	21:10	21:04	21:54	both
20110805	17:23	17:21	17:51	both
20120122	05:18	05:15	06:12	both
20120714	17:27	17:27	18:10	both
20121008	04:31	04:31	05:17	both
20121112	22:08	22:15	23:13	both
20121123	21:22	21:11	21:53	both
20130125	16:04	16:00	17:00	both
20130524	17:40	17:36	18:11	both
20130531	15:32	15:30	16:19	both
20130709	19:58	19:56	20:53	both
20140109	19:33	19:31	20:10	both
20140325	19:23	19:25	20:04	both
20140702	23:33	23:26	24:43	both
20150621	15:50	15:41	16:45	both
20150622	04:52	04:51	05:45	both
20150622	18:01	17:59	18:33	both
20151231	00:10	00:02	00:50	both
20160118	20:52	20:55	21:58	both
20160414	06:45	06:51	07:37	both
20180309	17:17	17:22	18:07	both
20190924	12:00	12:03	13:11	both
20201210	01:32	01:33	02:10	both
20211127	22:06	21:59	22:52	both
20220313	10:09	10:06	10:47	both
20000424	08:53	08:51	09:26	symH
20031106	18:56	19:19	19:41	symH
20050801	06:09	06:05	06:37	symH
20060815	16:26	16:24	17:26	symH
20110805	18:32	18:32	19:02	symH
20130718	12:49	12:41	13:32	symH
20131029	09:25	09:34	10:35	symH
20140706	09:51	09:41	11:05	symH
20150331	07:39	07:40	08:34	symH
20150624	13:01	12:57	13:28	symH
20211031	09:34	09:29	10:12	symH
19980504	02:36	02:29	02:57	weak
20010830	13:26	13:30	14:12	weak
20020826	10:19	10:46	11:32	weak
20050325[*2]	16:41	16:37	17:16	weak
20111112	05:10	05:18	06:00	weak
20120503	00:59	01:16	02:19	weak
20171217	06:36	06:33	07:24	weak

*1: Identification of geomagnetic SC by both methods (=2), by only SYM-H (=1), and weak/unclear SC (=?)

*2: Reverse (rarefied) shock

https://doi.org/10.5194/egusphere-2026-1517
Preprint. Discussion started: 21 April 2026

Table A4 Timing of IP detection and geomagnetic SC for SOHO-only 63 samples

Date	SOHO	SYM-H	SC[*1]
19960408	12:33	13:35	both
19970110	00:21	01:05	both
19970209	12:42	13:22	both
19970515	00:55	02:00	both
19970902	22:03	23:00	both
19971001	00:19	00:59	both
19971023	07:01	08:06	both
19971024	10:19	11:16	both
19971106	22:06	22:49	both
19971122	08:54	09:50	both
19971210	04:22	05:27	both
19971230	01:17	02:10	both
19980106	13:18	14:17	both
19980124	04:48	05:30	both
20000714	15:05	15:32	both
20000715	14:18	14:37	both
20001110	06:00	06:27	both
20010925	19:51	20:25	both
20011106	01:20	01:52	both
20011124	05:33	05:55	both
20040106	19:24	19:51	both
20050515	02:19	02:38	both
20050713	04:27	05:13	both
20050717	01:23	01:36	both
20050911	00:49	01:14	both
20110925	11:12	11:46	both
20120124[*2]	14:33	15:04	both
20120308	10:53	11:04	both
20130822	18:41	19:26	both
20141101	06:20	07:06	both
19960206	19:02	19:50	symH
19970111	04:27	05:16	symH
19970520	04:46	06:02	symH
19970903	08:11	08:56	symH
19971109	21:51	22:54	symH
19990628	02:28	02:59	symH
20000917	15:19	16:00	symH
20010118	09:18	10:12	symH
20030217	22:55	23:26	symH
20040122[*2]	08:45	09:22	symH
20040126	18:34	19:21	symH
20050429	15:31	16:06	symH
20050529	20:51	21:29	symH
20081028	19:44	20:10	symH
20160311	04:45	05:34	symH
20160725	01:15	02:12	symH
20220519	13:31	13:56	symH
19980131	15:56	16:44	weak
19980325	15:33	16:33	weak
19991204	00:47	01:31	weak
20000427	20:01	21:06	weak
20020326[*2]	10:13	10:50	weak
20030127	16:35	16:59	weak
20030311	15:46	17:16	weak
20030714	10:42	11:18	weak
20030726	12:36	13:06	weak
20031122	09:59	10:29	weak
20050508	09:07	09:34	weak
20061208	04:11	04:36	weak
20100908	01:07	02:18	weak
20150206	07:40	08:02	weak
20160311[*2]	19:18	19:47	weak
20201023	16:03	16:51	weak

*1: Identification of geomagnetic SC by both methods (=2), by only SYM-H (=1), and weak/unclear SC (=?)
*2: Reverse (rarefied) shock